Journal of the Mechanical Behavior of Biomedical Materials 97 (2019) 385–395

Contents lists available at ScienceDirect

Journal of the Mechanical Behavior of Biomedical Materials

journal homepage: www.elsevier.com/locate/jmbbm

Physical, mechanical properties and antimicrobial analysis of a novel $CaO{\cdot}Al_2O_3$ compound reinforced with Al or Ag particles

Sandra G. Gómez de Saravia[a], Silvia E. Rastelli[a], Mayahuel Ortega-Avilés[b], Carlos O. González-Morán[c], Enrique Rocha-Rangel[d], José G. Miranda-Hernández[c,*]

[a] Centro de Investigación y Desarrollo en Tecnologías de Pinturas (CIDEPINT), (CICPBA-CONICET-UNLP), Facultad de Ciencias Naturales y Museo, UNLP, La Plata, Buenos Aires, Argentina
[b] Instituto Politécnico Nacional, CNMN, Ciudad de México, Mexico
[c] Universidad Autónoma del Estado de México, Centro Universitario UAEM Valle de México, Laboratrorio de Investigación y Desarrollo de Materiales Industriales, Atizapan de Zaragoza, Estado de México, Mexico
[d] Universidad Politécnica de Victoria, Departamento de Manufactura de Materiales Avanzados, Ciudad Victoria, Tamulipas, México de postgrado, Ciudad Victoria, Tamaulipas, Mexico

ARTICLE INFO

Keywords:
Calcium aluminate-metal
Metallic particles
Snail shell powder
Solid state reactions
Mechanical properties
Antimicrobial analysis

ABSTRACT

Ceramic-metal ($CaO{\cdot}Al_2O_3$–Al and $CaO{\cdot}Al_2O_3$–Ag) compounds were prepared by mechanical milling and consolidated through an *in-situ* sintering process. The aim of this work is to study the effects of the Al and Ag particles to ceramic-base compound, primarily in the microstructure, and its mechanical and antimicrobial properties. Chemical systems with a 1:1 M ratio between $CaCO_3$ and Al_2O_3 powder were formed, with the addition of 10 wt% Al or 10 wt% Ag, respectively. The compound material that consolidated were microstructurally characterized through X-ray diffraction, scanning electron microscopy, optic microscopy, and X-ray computed tomography. In addition, the hardness, the fracture toughness, the transversal elastic modulus, and the antimicrobial property were evaluated. The results of X-ray diffraction identified the formation of the calcium aluminate phases, such as $CaO{\cdot}6Al_2O_3$ (hibonite:CA6), $CaO{\cdot}2Al_2O_3$ (grossite:CA2), and $CaO{\cdot}Al_2O_3$ (krotite:CA); as well as Al and Ag were identified in its respective system. In addition, the mechanical properties show changes compared to the reference material that was synthesized under the same conditions and, finally, these materials also have an antimicrobial effect, against the *Staphylococcus* bacterium that is common in the oral cavity, when studied in synthetic saliva.

1. Introduction

The ceramics nowadays have many industrial applications; for example, in the aeronautic industry, naval industry, military industry, sports industry, automotive industry, medical industry, and others. In especially the calcium aluminate $CaO{\cdot}Al_2O_3$ is a ceramic material with a considerable importance due to its several applications, such as a refractory material (Miranda Hernández et al., 2018), concrete-based calcium aluminate cement (Scrivener et al., 1999), catalyst (Zabeti et al., 2009), and metallurgical processes (Jiangling et al., 2015; Jifang et al., 2012, 2016). Also, this material has been studied for biomedical applications (Regina de Oliveira et al., 2015), such as in odontology (Leal Silva et al., 2014; Engqvist et al., 2004; Parreira et al., 2016; Loof et al., 2003; Oliveira et al., 2010; Andrade et al., 2014), bone replacement (Uchida et al., 1984) and bone-graft applications (Kalita et al., 2002; Hulbert et al., 1970). As well, calcium aluminate has been the focus of several studies about of the synthesis processes, such as the sol-gel method (Aitasalo et al., 2002), solid state reaction (Miranda Hernández et al., 2018; Aitasalo et al., 2002; Yongpan et al., 2016), sintering (Miranda Hernández et al., 2018; Iftekhar et al., 2008; Rivas et al., 2005), mechanochemical synthesis (Wieczorek-Ciurowa et al., 2010), and the sonochemical process (Lourençoa et al., 2013). Calcium aluminate is synthesized principally from the CaO and Al_2O_3 (Andrade et al., 2014; Yongpan et al., 2016; Iftekhar et al., 2008; Rivas et al., 2005; Wieczorek-Ciurowa et al., 2010; Lourençoa et al., 2013; Zawrah and Khalil, 2007), but in some cases, the CaO is obtained through the thermic effect from $CaCO_3$ (Miranda Hernández et al., 2018; Andrade et al., 2014; Iftekhar et al., 2008; Rivas et al., 2005; Galan et al., 2013). Also, $CaCO_3$ can be obtained from natural sources such as snail shells, egg shells or clam shells (Miranda Hernández et al., 2018; Singh and

* Corresponding author. Blvd. Universitario S/N predio San Javier, Pedregal de Atizapán, C.P. 52948, Atizapán de Zaragoza, Estado de México, Mexico.
E-mail address: jgmirandah@uaemex.mx (J.G. Miranda-Hernández).

https://doi.org/10.1016/j.jmbbm.2019.05.041
Received 18 January 2019; Accepted 27 May 2019
Available online 29 May 2019

Purohit, 2010; Viriya et al., 1016; Ligaszewski et al., 2009; White et al., 2007; Marxen et al., 2003; Niju et al., 2016). Microstructure and mechanical properties of the calcium aluminate $CaO{\cdot}Al_2O_3$ were studied in our previous work. Considering the temperature effect during the synthesis process (Miranda Hernández et al., 2018), it was found that the calcium aluminate material synthesized by an *in-situ* solid state reaction between Al_2O_3 and $CaCO_3$ obtained from snail shells is feasible, but the results show that this material is brittle. However, there are several investigations showing that the incorporation of metallic or ceramic particles into the matrix of the ceramic materials modified their physical properties and mechanical properties, such as hardness, fracture toughness, elastic modulus, and fatigue strength (Naga et al., 2019; Tahaa et al., 2017; Granados et al., 2017; José et al., 2016; Sergejev and Antonov, 2006; Moradkhani et al., 2013; Pramanick, 2015; González-Morán et al., 2017; Shukla et al., 2010; Dapievea et al., 2018). In other works, the effect of silver particles with calcium aluminate was studied and it was found that with silver particles, calcium aluminate has favorable conditions as an endodontic sealer, that presents improved antibiofilm properties with a positive effect on antimicrobial behavior (Almeida et al., 2018). Also, there are studies that show that the calcium aluminate cement is a material with suitable biological and physicochemical properties as endodontic material due to the suitable cytotoxicity, physicochemical properties and the antimicrobial capability (Leal Silva et al., 2014; Andrade et al., 2014).

Therefore, this study has the purpose to establish a direct fabrication route of ceramic compounds with the addition of metallic particles by an *in-situ* process. The synthesis of this material considers the obtaining of $CaCO_3$ from snail shells as a source of CaO to get calcium aluminates (Miranda Hernández et al., 2018; Aitasalo et al., 2002; Galan et al., 2013; Singh and Purohit, 2010; Viriya et al., 1016). On the other hand, the selection of Al and Ag as reinforcement metals in the ceramic matrix has two intentions; the first, it is to study the effect of the metallic particles on the microstructure and its mechanical properties, such as hardness, fracture toughness, and shear modulus considering that Al and Ag are ductile and malleable metals; the second, is a study of the biological behavior considering some medical application principally as dentistry material (Regina de Oliveira et al., 2015; Leal Silva et al., 2014; Engqvist et al., 2004; Oliveira et al., 2010; Andrade et al., 2014; Aguilar et al., 2012).

2. Material and methods

2.1. Synthesis process

The raw material used for the synthesis of the ceramic compound were α-Al_2O_3 powder (≥98% purity, < 100 mesh, Aldrich), Al powder (≥99% purity, < 200 mesh, Aldrich), Ag powder (≥99% purity, < 200 mesh, Aldrich), and $CaCO_3$ (<100 mesh) from the snail shells (Miranda Hernández et al., 2018). With a 1:1 M relation between Al_2O_3 and $CaCO_3$ powder, three chemical systems were formed: Al_2O_3/49.54 wt% $CaCO_3$, Al_2O_3/49.54 wt% $CaCO_3$ + 10 wt% Al, and Al_2O_3/49.54 wt% $CaCO_3$ + 10 wt% Ag. The powder mixtures were submitted through a mix-milling process (Fritsch, Pulverisette 6) for 4 h and 200 rpm with a 1:10 ratio of balls-milling into a container of the agate. The powder mixtures then were compacted into cylindrical samples using a uniaxial load of 300 MPa at room temperature and these compacted materials were sintered in an electrical furnace (Nabertherm, LHT 02/18) in an argon atmosphere. The compacted materials were submitted through a sintering process with a heating rate of 10 °C/min considering that the temperature was elevated at 400 °C, then, increased to 800 °C and 1200 °C (each step was stabilized for 20 min). Finally, the samples were kept at 1500 °C for 60 min.

2.2. Microstructural characterization

The microstructure was observed through an optical microscope (Olympus, GX51), scanning electron microscope (JEOL, JSM6300) equipped with an energy-dispersive X-ray spectrometer (EDX) and X-ray computed tomography (Industrial X-ray equipment, XTH225). The structural analysis was carried out by X-Ray diffraction (XRD) (Panalytical, X'PertPRO) with Cu radiation (λCu = 1.54056 Å) operating at 40 KV and 40 mA and a range of 2 theta of 15–100 grades with a step of 0.02 grades.

2.3. Physics and mechanical properties

The bulk density and the porosity were determined by the Archimedes' method (ASTM: B962-13). Likewise, the mechanical properties such as hardness and fracture toughness (K_{IC}) were determined using the Vickers Indentation technique (Emco-Test, DuraScan 20) (Miranda Hernández et al., 2018; Tahaa et al., 2017) and the transversal elastic modulus (shear modulus) was determined by an ultrasonic method (Phase II Machine & Tool, UTG-2800) (Miranda Hernández et al., 2018; Gondard et al., 1998), according to relation $G = \rho\varepsilon^2$, where G is the shear modulus, ρ is the bulk density, and ε is the transversal sound velocity measured in the synthesized materials.

2.4. Microbiological analysis

The materials synthesized were submitted to an antimicrobial sensitivity test against the bacterium *Staphylococcus* sp., common in the oral cavity (Leal Silva et al., 2014; Friedlander, 2010; Smith et al., 2001; Tsang et al., 2002). From a fresh culture of Staphylococcus, 120 ml of a liquid suspension was prepared in synthetic saliva B broth (NaCl: 6 g/l, KCl: 0.3 g/l, $CaCl_2$: 0.2 g/l, lactic acid: 3.1 g/l, Na_2SO_3: 0.1 g/l, thioglycolic acid: 0.5 g/l, yeast extract: 0.5 g/l and glucose: 1 g/l, pH ≈ 6.5) with an $DO_{600} \approx 0.1$ ($\approx 10^8$ UFC ml^{-1}). The samples were sterilized in UV for 30 min, then were submerged and suspended in the culture for 48 h of incubation at 28 ± 2 °C under sterile conditions. Afterwards, one side of the sample with the biofilm was left attached and the other half was cleaned with a sterile swab. The samples were fixed in 2.5% glutaraldehyde, dehydrated in increasing concentrations of ethanol, dried by critical point and metalized for observation by scanning electron microscopy (FEI, Quanta 200).

3. Results and discussion

3.1. Synthesis

$CaCO_3$ used as raw material in the synthesis process obtained from snail shells was analyzed by DRX analysis, the results identified that this material is $CaCO_3$ in the aragonite and calcite phases. The obtaining process and analysis of this material were reported by us in a previous investigation (Miranda Hernández et al., 2018). The chemical systems previously formed were compacted in cylindrical samples and then were sintered. After the sintering process, the samples showed an important change in the mass, as is reported in Table 1.

The mass loss is due to the chemical decomposition of the $CaCO_3$ to CaO and CO_2 by temperature effect during the sintering process (635–865 °C) (Miranda Hernández et al., 2018; Yongpan et al., 2016; Iftekhar et al., 2008; Rivas et al., 2005; Galan et al., 2013), according to Eq. (1).

Table 1
Average mass of the materials before and after sintering process.

Material	Al_2O_3 + $CaCO_3$	(Al_2O_3/$CaCO_3$) + Al	(Al_2O_3/$CaCO_3$) + Ag
Initial mass (g)	2.479	(2.223) + 0.247	(2.243) + 0.249
Final mass (g)	1.779	(1.617) + 0.247	(1.626) + 0.249
Mass loss (g)	0.700 (~28.2%)	0.606 (~27.3%)	0.617 (~27.5%)

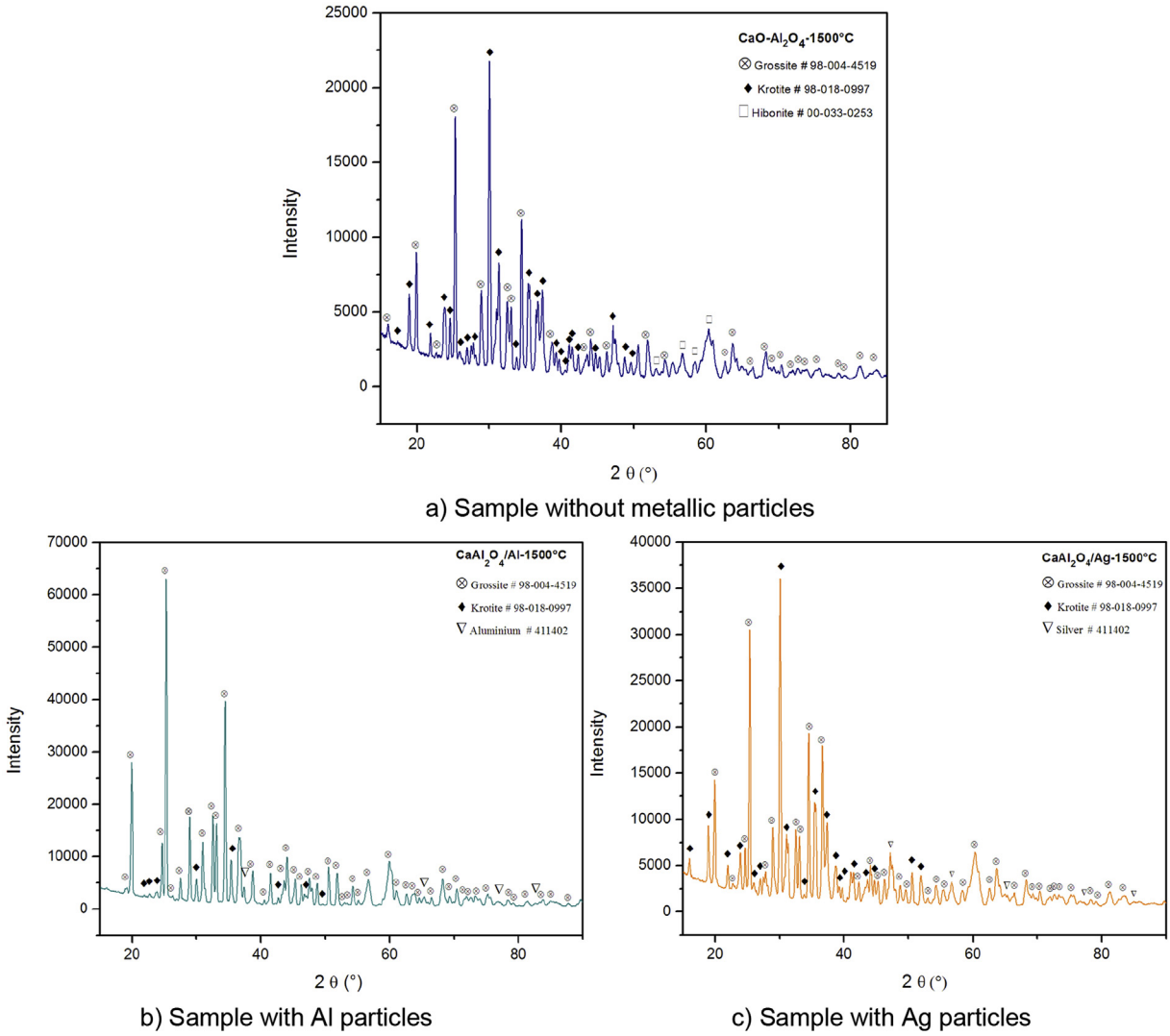

Fig. 1. XRD pattern of samples sintered with and without metallic particles.

$$Al_2O_3 + CaCO_3 \xrightarrow{\Delta} Al_2O_3 + CaO + CO_2\uparrow \quad (1)$$

Also, during the sintering process, when the temperature continued to increase up 1500 °C and just after the decomposition of the calcium carbonate, a continued *in-situ* solid state reaction occurred between Al_2O_3 and CaO for the formation of the calcium aluminate, according to Eq. (2) (Miranda Hernández et al., 2018; Yongpan et al., 2016; Iftekhar et al., 2008; Rivas et al., 2005; Galan et al., 2013).

$$Al_2O_3 + CaO \xrightarrow{\Delta} CaAl_2O_4 \quad (2)$$

In the cases of the chemical compositions with the metallic particles according to Eq. (3) and Eq. (4), only the Al_2O_3 and CaO have a chemical reaction forming a ceramic-metal compound as calcium aluminate-Al and calcium aluminate-Ag.

$$Al_2O_3 + CaCO_3 + Ag \xrightarrow{\Delta} CaAl_2O_4 + Al \quad (3)$$

$$Al_2O_3 + CaCO_3 + Ag \xrightarrow{\Delta} CaAl_2O_4 + Ag \quad (4)$$

On the other hand, the synthesis of these materials is based on the experimental chemical reactions previously described and reported in other works (Miranda Hernández et al., 2018; Yongpan et al., 2016; Iftekhar et al., 2008; Rivas et al., 2005; Galan et al., 2013). Due to that, the thermic analysis was not considered in this work. But, the synthesis of the calcium aluminate material and calcium aluminate - metal compounds by XRD and EDS analysis were confirmed.

3.2. X-ray diffraction analysis

The mass loss in the chemical systems during the sintering process is the evidence of the decomposition of $CaCO_3$ to CaO for its posterior reaction with Al_2O_3 for the formation of calcium aluminate. Namely, the XRD analysis shows the absence of Al_2O_3 and CaO that confirm the total reaction between Al_2O_3 and CaO during the sintering process, as is shown in Fig. 1. In particular, the XRD patterns of Fig. 1 (a) several phases were identified corresponding to calcium aluminates, such as $CaO{\cdot}2Al_2O_3$ (CA2: Calcium di-aluminate: Grossite), $CaO{\cdot}Al_2O_3$ (CA: Calcium mono-aluminate: Krotite), and $CaO{\cdot}6Al_2O_3$ (CA6: Calcium hexa-aluminate: Hibonite). However, the formation of several phases of calcium aluminates is due to the fact that the initial chemical components donot have a uniform distribution during the mix-milling process, and considering that the time spent in this process is little (4 h) that causes rich zones of Al_2O_3 in the compacted materials. For example, the CA6 phase formed during the sintering process is due to the presence of rich zones of Al_2O_3 in the system or punctual zones with the least amount of CaO, that favors the formation of this phase during the sintering process according to Eq. (5) (Miranda Hernández et al., 2018; Yongpan et al., 2016; Iftekhar et al., 2008; Miskufova et al., 2015).

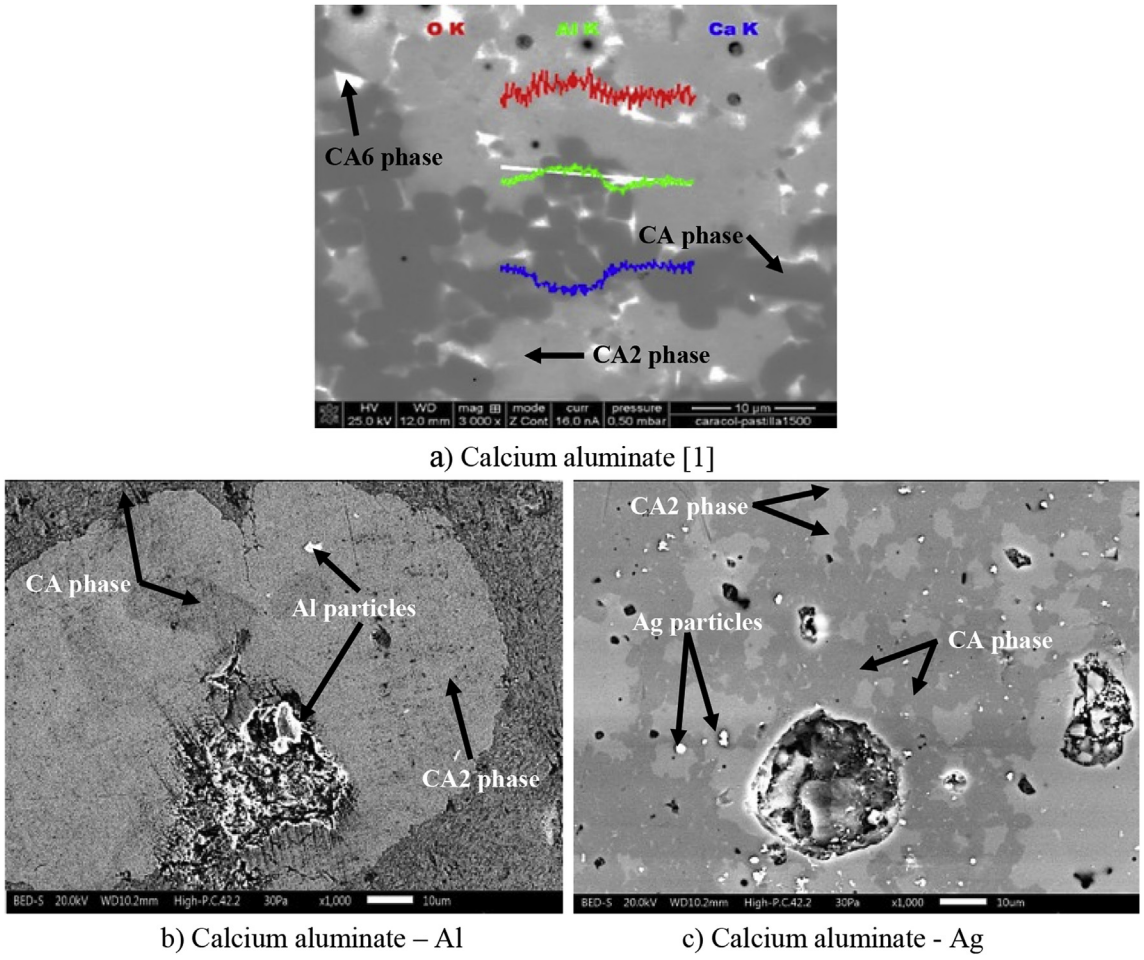

Fig. 2. Backscattered electron image.

$$6Al_2O_3 + CaO \xrightarrow{\Delta} CaAl_{12}O_{19} \quad (5)$$

Therefore, taking up again thermodynamic data reported by some authors (Miskufova et al., 2015; Rivas et al., 2005; Eliezer et al., 1981), the first phase formed during the sintering process must be the hibonite phase (CA6), which is richer in Al_2O_3 content; after this, grossite (CA2), and krotite (CA) are formed (Miranda Hernández et al., 2018; Yongpan et al., 2016; Iftekhar et al., 2008; Rivas et al., 2005). While, according to DRX analysis, the CA6 phase was only identified in the materials synthesized without metallic particles (see Fig. 1), although the XRD analysis also identified Al and Ag respectively.

3.3. Microstructure

Fig. 2 (a) shows the backscattered electron image. Based on an elemental profile it is possible to identify the variation of the concentration of Al and Ca in a zone with different contrast. With the combination of the XRD analysis and elemental profile by EDS, it is possible to affirm that the clear, medium, and darker gray zones correspond to CA6, CA2, and CA phases respectively. Fig. 2 (b) and (c) of the material synthesized with Al and Ag additions only exhibits the phases identified as CA2 and CA, meanwhile, the CA6 phase was not found in these materials.

The sintered samples were also analyzed through optic microscopy; these microstructures are shown in Fig. 3. The microstructure corresponding to pure calcium aluminate (see Fig. 3 (a) and (b)), presents only one phase corresponding to the matrix of the ceramic material and also its porosity. Fig. 3 (c) and (d) show the microstructure of the calcium aluminate with Al. In this microstructure, the matrix material is notable as well as the presence of the Al metallic particles. In a similar analysis, Fig. 3 (e) and (f) show the matrix of the ceramic material and the Ag particles added in the system during the synthesis process.

The porosity of these materials has a peculiar behavior, since the porosity in the pure material is similar to that of the ceramic compounds with Al and Ag. It should be noted that the porosity of this material is not homogeneous considering that pores of irregular shapes are observed, others with hemispherical shape or long pores (cavities) in the case of material with Ag (Fig. 3)". The formation of the porosity is a peculiar characteristic of this manufacturing process and it is also the consider that during the sintering process the $CaCO_3$ is decomposed to CaO and CO_2 (gas), where the gas is liberated from the system which results in the production of pores during the liberation.

On the other hand, the distribution of metallic particles in the matrix of the ceramic material is an important characteristic to consider. Due to this fact, the metallic particles have an effect in the physics and mechanical properties. Taking this consideration, the calcium aluminate material with Ag was submitted to X-ray computed tomography, as is shown in Fig. 4. In this figure, it is notable that the Ag particles are distributed in the ceramic material on the transversal and longitudinal profiles, respectively. Due to that the software of the XRD-CT equipment eliminating the ceramic phase, the right image only shows the distribution of the metallic particles in the system.

Considering that the sintering process was carried out in the presence of a one liquid phase and the effect of the diffusion phenomena, the metallic particles are distributed and agglomerated in all ceramic material caused by the temperature used in the sintering process. For this to happen, the metallic particles begin and begin well distributed in the matrix of the ceramic material, but when the metallic particles are

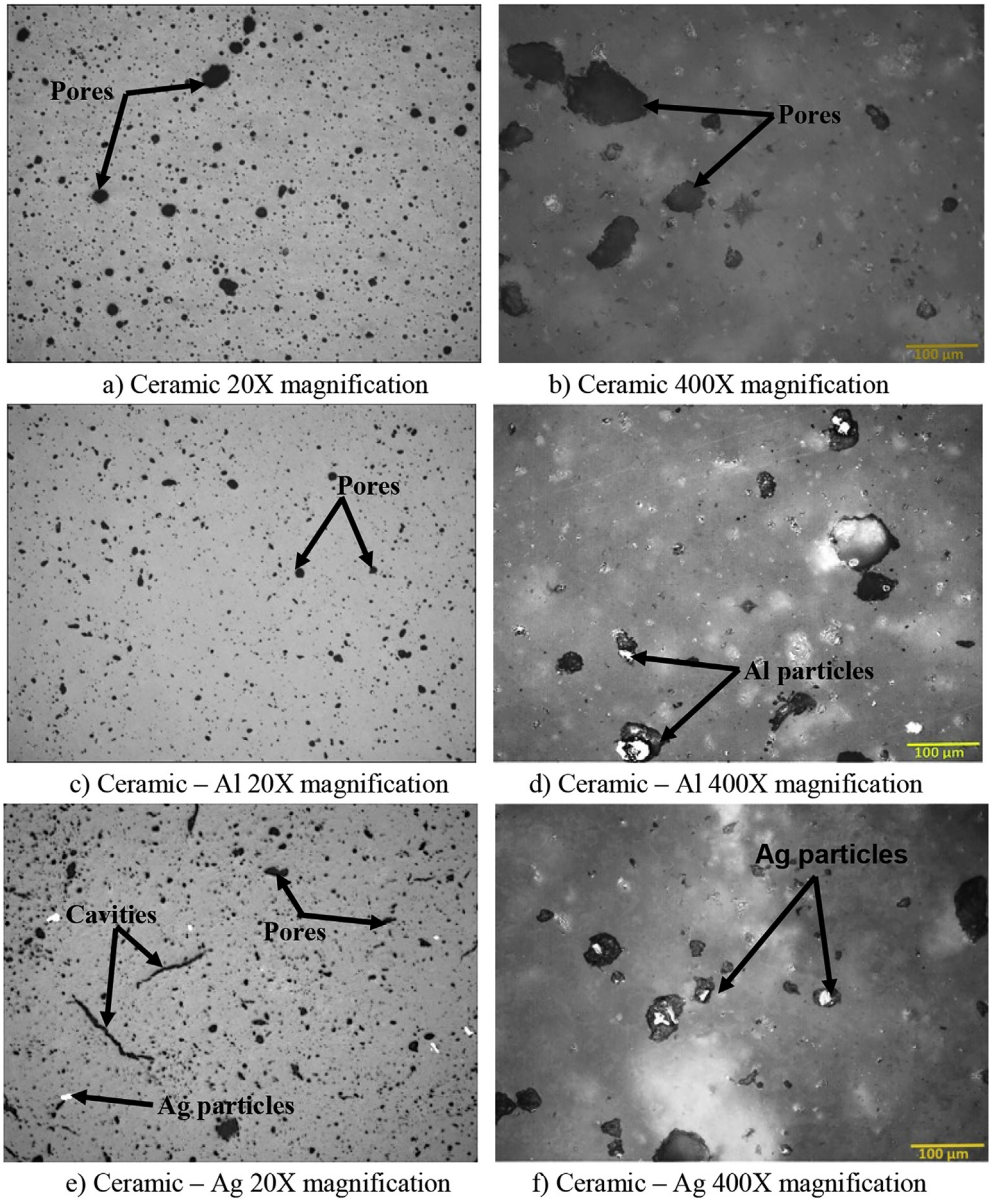

Fig. 3. Microstructures by optic microscopy of the sintered materials without metallic particles and with metallic particles.

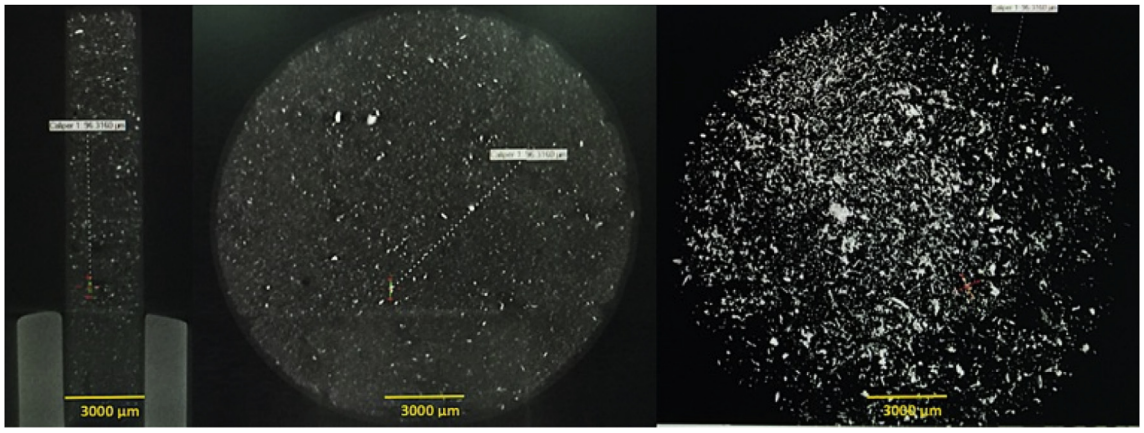

Fig. 4. X-ray CT of sintered calcium aluminate sample with Ag.

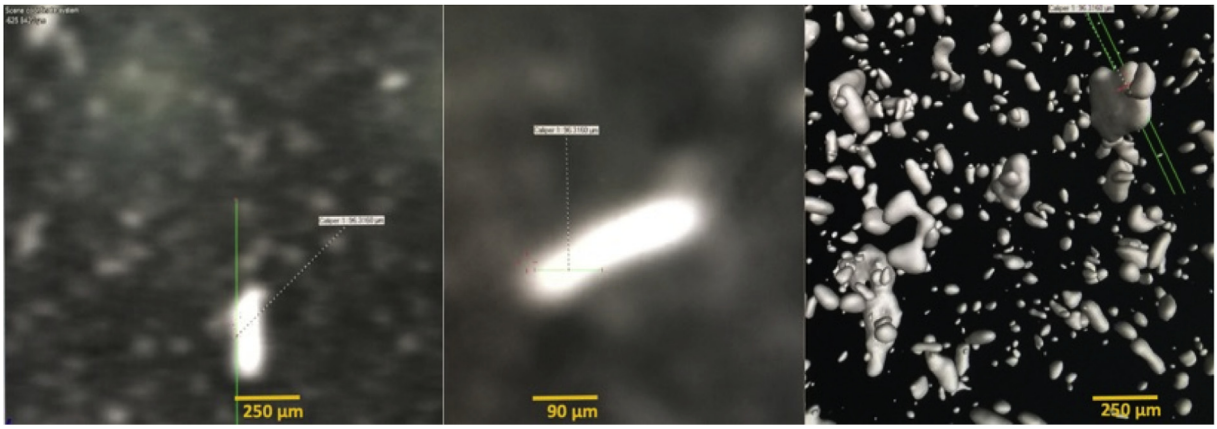

Fig. 5. X-ray CT of sintered calcium aluminate material with Ag.

Table 2
Physics properties of compound materials.

Properties	Calcium Aluminates		
	Without Metals	With Al	With Ag
Bulk density (g/cm^3)	2.88	2.98	3.66
Densification (%)	94.1	93.9	92.7
Apparent (open) porosity (%)	~3.0	~3.1	~3.4
Volumetric shrinkage (%)	49.5	47.9	46.7

Table 3
Mechanical properties of compound materials.

Properties	Calcium Aluminates		
	Without Metal	With Al	With Al
Hardness (GPa)	8.4 ± 0.2	11.4 ± 0.5	9.3 ± 0.3
Fracture toughness (Kic/MPa·m$^{1/2}$)	0.43 ± 0.07	1.72 ± 0.28	1.26 ± 0.19
Shear modulus (GPa)	55 ± 2	64 ± 1	69 ± 1

agglomerated, the particles increase in size and take a different form. Namely, the initial size of the Ag particles was of the order of < 74 µm (< 200 mesh) on average and after the sintering process, the particles sizes increased to a size bigger than 75 µm, as is shown in Fig. 5. Finally, in the images of Figs. 2, 3 and 5, it is possible to observe that the size of silver particles is of the order between a 1 µm and may be to 250 µm.

3.4. Physics properties

The physics properties of the materials manufactured are reported in Table 2. These values indicate a bulk density of 2.88 g/cm^3 (94.1 densification %) for pure calcium aluminate, 2.98 g/cm^3 (93.9 densification %), and 3.66 g/cm^3 (92.7 densification %) for the compound materials with Al and Ag, respectively. The reason why the density increases is due to the incorporation of a material with major density in the ceramic system as Al (2.7 g/cm^3) and Ag (10.49 g/cm^3). However, at the same time, the densification percent has a diminution that is related with the increases of the apparent porosity percent in the ceramic materials without and with metals, respectively, the apparent porosity percent values are reported in Table 2. In another work, it was found inverse comportment. Namely, while the densification percent increases, the apparent porosity decreases (Tahaa et al., 2017). A possible reason that the compound material with Ag has a minor densification percent and major apparent porosity may be due to the shape of the pores, considering that there is a presence of long pores (see Fig. 3 (e)). On the other hand, the densification percent and porosity are also related with the changes in the volumetric shrinkage (see Table 2). As expected, the volumetric shrinkage of the calcium aluminate is 49.5%, which is higher than 47.9% and 46.7% determined for the materials with Al and Ag, respectively.

3.5. Mechanical properties

The physics comportment has an effect in the mechanical properties, such as hardness, fracture toughness (K_{IC}), and shear modulus. The average values of the mechanical properties are reported in Table 3. It was found that the materials synthesized without metallic particles and with metallic particles as Al and Ag have hardness values of 8.4 ± 0.2 GPa, 11.4 ± 0.5 GPa and 9.3 ± 0.3 GPa, respectively. In comparison to pure calcium aluminate material, the increases in the compounds' hardness are attributed to the presence of metallic particles that it has as a reinforcement function in the ceramic matrix, but it is also related to the behavior of bulk density. In other investigations, it was found a similar behavior when a ceramic material is reinforced with a secondary phase (Naga et al., 2019; Tahaa et al., 2017).

The fracture toughness was determined using some theoretical and empirical mathematical models proposed by Lawn-Evans-Marshall (Lawn et al., 1980), Lawn-Fuller (Lawn and R Fuller, 1975), Evans-Charles (Evans and Charles, 1976), Anstis-Chantikul-Lawn-Marshall (Anstis et al., 1981), Japanese International Standard (JIS) (JSA - JIS R 1607, 1990), and Niihara-Morena-Hasselman (Niihara et al., 1982). The values determined by each mathematical model in each material have a similar tendency as is shown in Fig. 6. The values reported in Table 3 are the average values of the fracture toughness of the materials determined by each mathematical model. Namely, the calcium aluminate synthesized with metallic particles such as Al and Ag has average values of 1.72 ± 0.28 MPa m$^{1/2}$ and 1.26 ± 0.19 MPa m$^{1/2}$, respectively. These values are higher than 0.43 ± 0.07 MPa m$^{1/2}$ of the calcium aluminate without metallic particles. As it is known, if the fracture toughness value is low in the materials, then the material is susceptible to mechanical flaws due to its fragility. In consideration, when the metallic particles such as Al and Ag melt during the sintering process, the metallic particles are agglomerated and distributed in the matrix of the ceramic material. Therefore, this is the reason why the fracture toughness increases in comparison with the pure calcium aluminate, that is, the presence of metallic particles in the ceramic matrix limits the propagation of cracks. Thus, the increase in metallic inclusions affects the crack propagation path due to there existing a high probability to collide with any Al or Ag particle that acts as barriers and promotes the crack to stop (Tahaa et al., 2017). The cracks can have a loss of energy that prevents its growth because the metal particle absorbs this energy, forcing the cracks to move around the inclusions, increasing the fracture toughness (Naga et al., 2019; Tahaa et al., 2017; José et al., 2016).

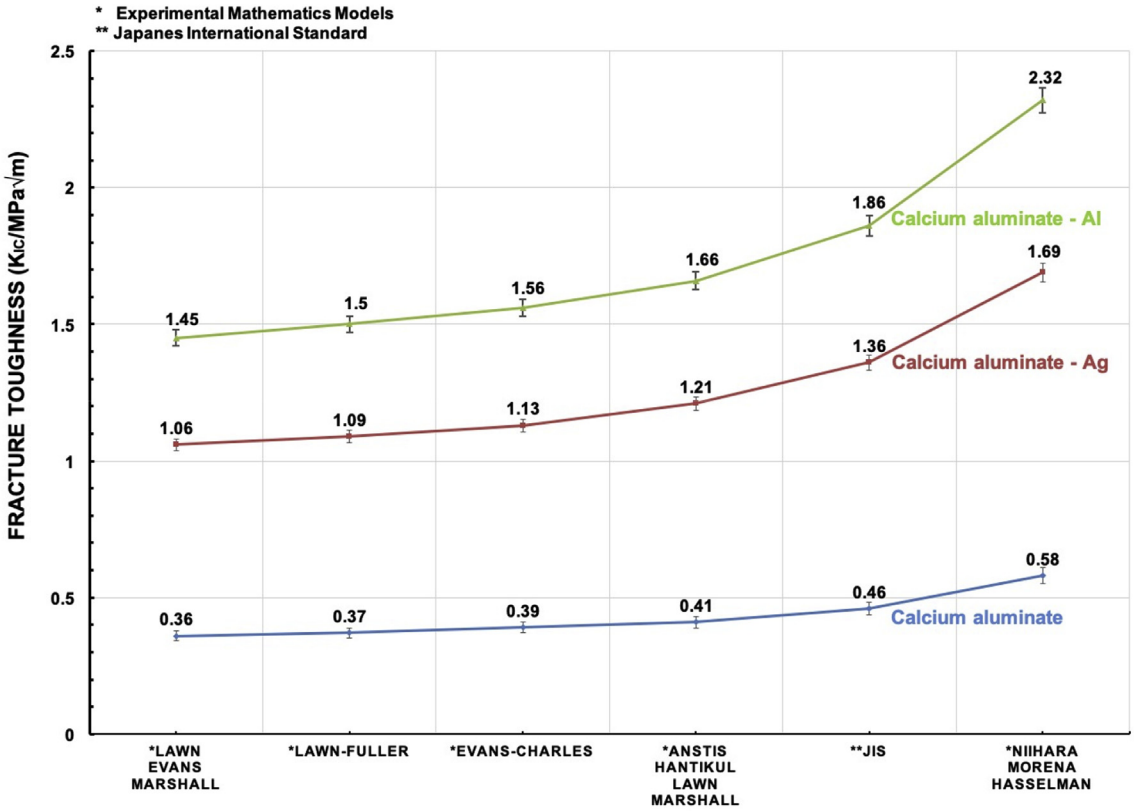

Fig. 6. Fracture toughness of the synthesized materials.

Finally, the shear modulus or transversal elastic modulus determined in the synthesized materials are 55 ± 2 GPa, 64 ± 1 GPa and 69 ± 1 GPa for pure calcium aluminate, calcium aluminate-Al and calcium aluminate-Ag, respectively (see Table 3). Naturally, the inclusions of the metallic particles into the ceramic matrix has effect in this elastic property due to that these particles are of softer characteristics compared with based material (Tahaa et al., 2017), although is expected that, if the shear modulus decreases, the fracture toughness increase. This behavior is observed in the material compounds with Al and Ag, respectively, that is, the shear modulus for the calcium aluminate-Al compound is 64 ± 1 GPa lower than 69 ± 1 GPa of the calcium aluminate-Ag compound, but the fracture toughness in the calcium aluminate-Al is major than calcium aluminate-Ag. This behavior was observed in another study (Tahaa et al., 2017).

3.6. Antimicrobial analysis

The SEM microstructures, EDS analysis, and the metallization process were determined before of antimicrobial test, against the bacterium *Staphylococcus* sp. Fig. 7 shows the microstructural morphology and EDS analysis confirm the presence of the Al and Ag elements in the ceramic matrix (see Fig. 7 (b) and (c)). In addition, observe that bacterial growth is not notable on the surface of all materials according to the microstructures image.

Also, the drop contact angle on the surface of the synthesized materials was determined, as shown in Fig. 8. The information of this value is important because it is known that the drop contact angle on the surface of the materials has a relation with the hydrophilicity, and it is a factor that influences the bacterial adherence. In these surfaces, the values of the drop contact angle in all materials are $< 90^{\circ}$, the hydrophilicity does not have the influence on the bacterial adherence, considering that this physicochemical property is important in the biocompatibility of the materials.

As mentioned, Staphylococcus is a microorganism whose presence has been reported in the oral cavity (Leal Silva et al., 2014; Friedlander, 2010; Smith et al., 2001; Tsang et al., 2002). To analyze the biocidal characteristic of the materials under study, after 48 h of immersion in the culture medium with Staphylococcus sp, the samples were observed by SEM.

After the antimicrobial sensitivity test, it is possible to observe that the biofilm formed on the surface of all materials, as shown in Fig. 9(d–f), compared to the reference samples before the antimicrobial test (Figs. (a–c)). In Fig. 9 (d), it is notable that the pure calcium aluminate has a greater development of extracellular polymeric material (EPM). Conversely, the calcium aluminate-Ag material has an important decrease of the presence and bacterial adherence. This decrease could be attributed to the Ag, knowing that Ag has antifungal properties. Other researchers have also found that the presence of Ag in a calcium aluminate sealer have a bacterial biofilm inhibition compared to the same material without Ag particles (Almeida et al., 2018). In the case of the material calcium aluminate with Al, there is a bacterial adherence on the surface, but the adherence is less than pure calcium aluminate (Fig. 9 (e)).

The other side of the sample was cleaned with a sterile swab and was also metalized for its observation with the aim to analyze the possible deterioration caused by the microorganisms, as shown in Fig. 10. According to the time test, it is not possible to observe changes on the surface of the different materials due to the bacterial presence after the antimicrobial test. In others, similar studies with several bacteria including the *Staphylococcus* genus, it was found that the calcium aluminate-based endodontic material had good antimicrobial capability (Leal Silva et al., 2014; Aguilar et al., 2012).

4. Conclusions

A novel $CaCO_3 - Al_2O_3/Al$ and $CaCO_3–Al_2O_3/Ag$ ceramic compounds prepared by a solid-state reaction from a natural source of $CaCO_3$ is feasible using little time in the sintering process. During the

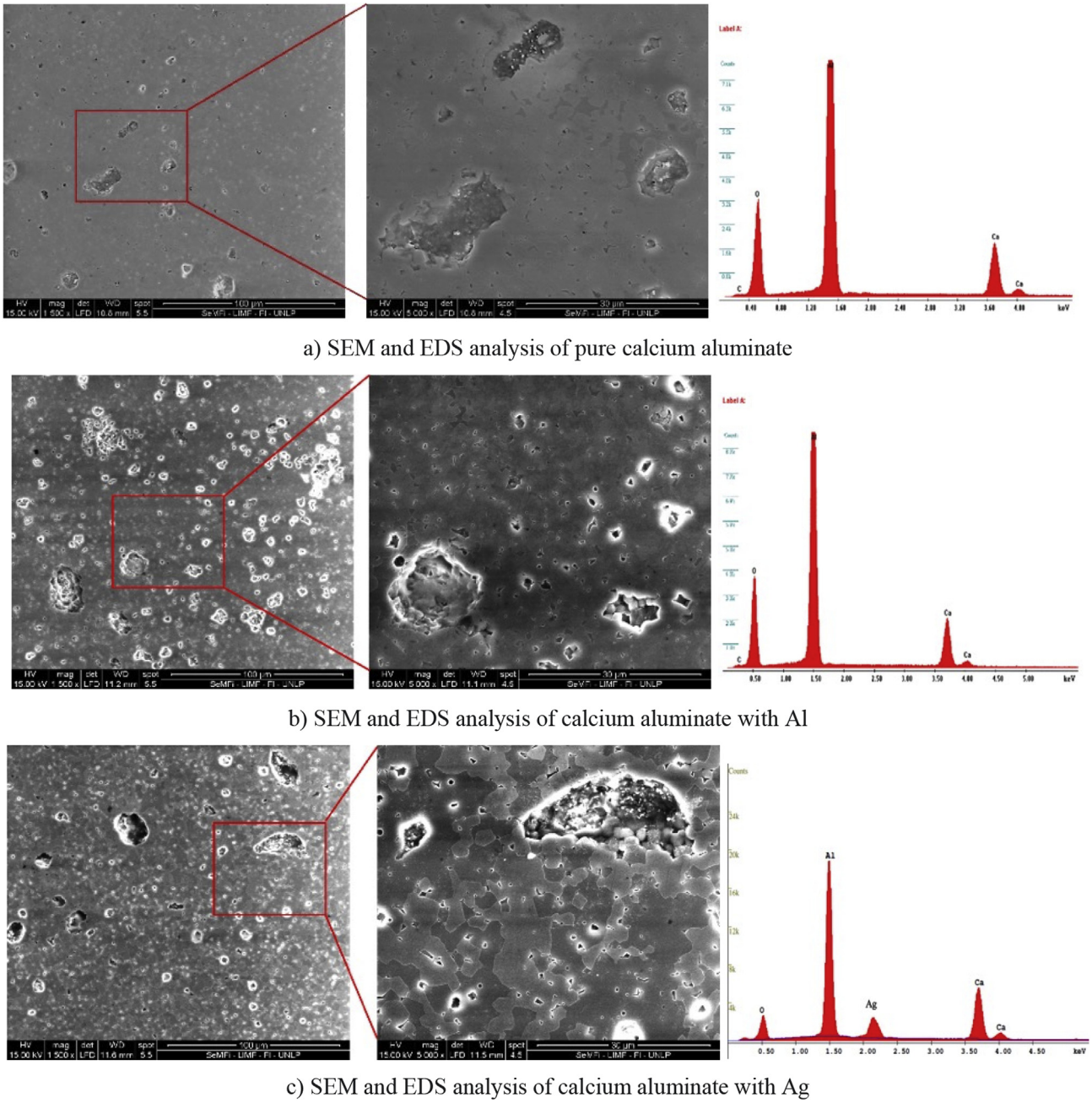

Fig. 7. Microstructures by SEM and EDS analysis of the sintered materials without metallic particles and with metallic particles.

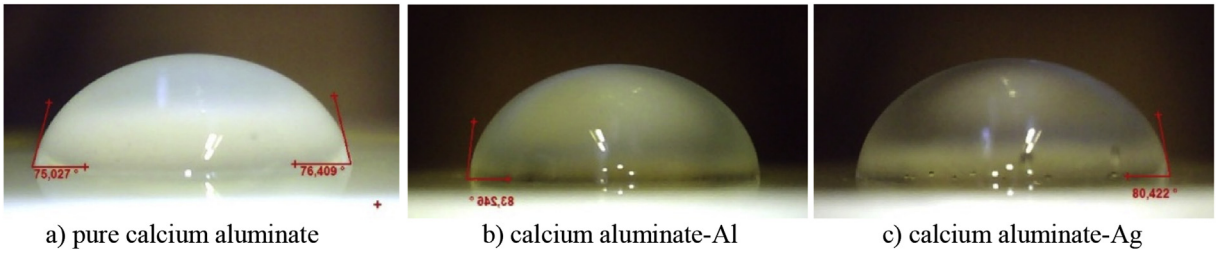

Fig. 8. Drop contact angle of the sintered materials.

heating process, $CaCO_3$ from snail shells has a chemical reaction with Al_2O_3 producing calcium aluminate - Al and calcium aluminate - Ag. The calcium aluminate is formed principally by three different phases, such as CA6: hibonite, CA2: grossite, and CA: krotite. The formation of the CA6 phase during the sintering process is due to that there being Al_2O_3-rich zones or micro-regions in the samples or because there are punctual zones with least amount of CaO. The CA6 phase does not appear in the material fabricated with Al and Ag.

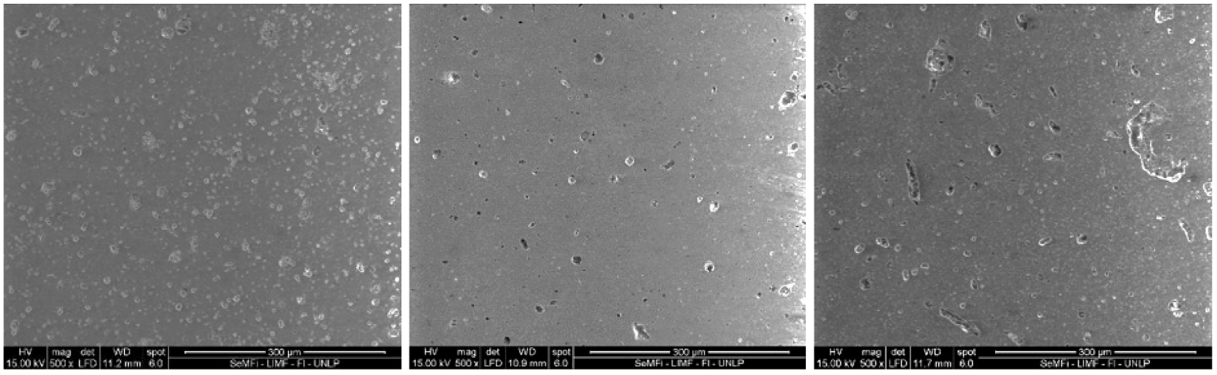

Fig. 9. SEM micrographics of the bacterial adherence on the surface materials with biofilm.

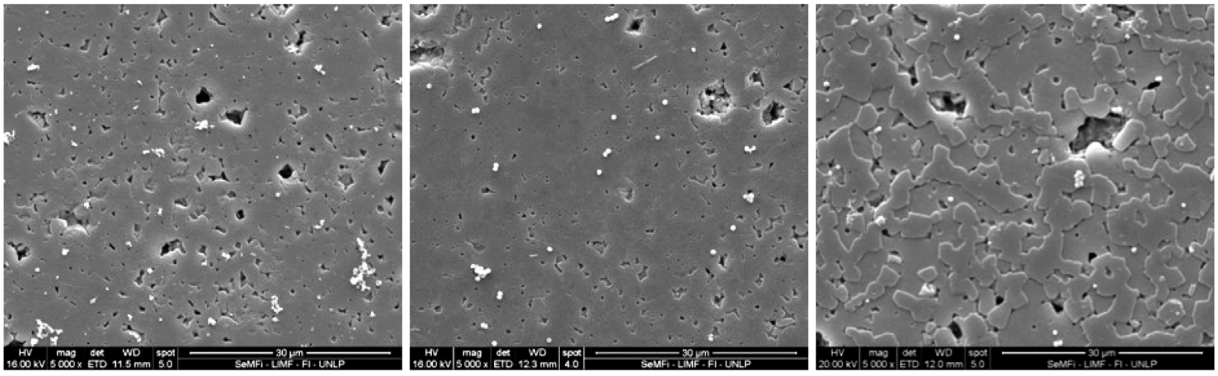

Fig. 10. SEM micrographics of the bacterial adherence on the surface materials without biofilm.

Calcium aluminate with Al addition is the material with better percent densification and Volumetric shrinkage. This same material has the major fracture toughness value compared with the pure material and calcium aluminate with Ag. Therefore, calcium aluminate - Al is the material with the best mechanical fracture conditions due to the effect of the addition of Al in the system. Although, this material has a disadvantage in reference with its antimicrobial conditions compared with the material with Ag particles.

The results support the idea that Ag particles incorporated into calcium aluminate ceramic may prevent the development of bacterial biofilms. The microbiological results indicate that calcium aluminate material with Ag particles would be useful as materials with anti-adherence activity.

Acknowledgments

The teamwork “Manufactura y Desarrollo de Materiales Multifuncionales” of the UAEM, CIMAV-Chihuahua and UPV, appreciates the collaboration and knowledge development and infrastructure between these Institutions. Also, researcher team UAEM-CA-202 gives thanks to PFCE 2019 program of the SEP for the support in the consolidation of this group. Also, part of this work was supported for the grants of National University of La Plata Project 11/I201, CONICET-PIP No. 00314 and CICBA 195/17. The authors thank to Eng. Pablo Seré (ANELPIRE-CIDEPINT) for the contact angle measurements.

Appendix A. Supplementary data

Supplementary data to this article can be found online at https://

doi.org/10.1016/j.jmbbm.2019.05.041.

References

Aguilar, F.G., Roberti Garcia, L.F., Pires de Souza, F.C.P., 2012. Biocompatibility of new calcium aluminate cement (EndoBinder). J. Endod. 8, 367–371. https://doi.org/10.1016/j.joen.2011.11.002. doi:.

Aitasalo, T., Hölsä, J., Jungner, H., Lastusaari, M., Niittykoski, J., 2002. Comparison of sol-gel and solid-state prepared $Eu2^{+}$ doped calcium aluminates. Mater. Sci. 20, 15–20.

Almeida, L.H.S., Moraes, R.R., Morgental, R.D., Cava, S.S., Rosa, W.L.O., Rodrigues, P., Ribeiro, A.S., Só, M., Pappen, F.G., 2018. Synthesis of silver containing calcium aluminate particles and their effects on a MT-Abased endodontic sealer. Dent. Mater. 34, 214–223. https://doi.org/10.1016/j.dental.2018.05.011.

Andrade, T.L., Santos, G.L., Pandolfelli, V.C., Oliveira, I.R., 2014. Synthesis otimization of calcium aluminate cement phases for biomedical applications. Cerâmica 60, 88–95. https://doi.org/10.1590/S0366-69132014000100013.

Anstis, G.R., Chantikul, P., Lawn, B.R., Marshall, D.B., 1981. A critical evaluation of indentation techniques for measuring fracture toughness: I, Direct crack measurements. J. Am. Ceram. Soc. 64, 533–538. https://doi.org/10.1111/j.1151-2916.1981.tb10320.x.

Dapievea, K.S., Guilardia, L.F., Silvestria, T., Rippea, M.P., Rocha Pereira, G.K., Valandroa, L.F., 2018. Mechanical performance of Y-TZP monolithic ceramic after grinding and aging: survival estimates and fatigue strength. J. Mech. Behav. Biomed. Mater. 87, 288–295. https://doi.org/10.1016/j.jmbbm.2018.07.041.

Eliezer, I., Eliezer, N., Howalt, R.A., Viswanadham, P., 1981. Thermodinamic properties of calcium aluminates. J. Phys. Chem. 85, 2835–2838. https://doi.org/10.1021/j150619a028.

Engqvist, H., Schultz-Walz, J.E., Loof, J., Botton, G.A., Mayer, D., Phaneuf, M.W., Ahnfelt, N.O., Hermansson, L., 2004. Chemical and biological integration of a mouldable bioactive ceramic material capable of forming apatite in vivo in teeth. Biomaterials 25, 2781–2787. https://doi.org/10.1016/j.biomaterials.2003.09.053.

Evans, A.G., Charles, E.A., 1976. Fracture toughness determinations by indentation. J. Am. Ceram. Soc. 59, 371–372. https://doi.org/10.1111/j.1151-2916. 1976.tb10991.x.

Friedlander, A.H., 2010. Oral cavity staphylococci are a potential source of prosthetic joint infection. Clin. Infect. Dis. 50, 1682–1683. https://doi.org/10.1086/653003.

Galan, I., Glasser, F.P., Andrade, C., 2013. Calcium carbonate decomposition. J. Therm. Anal. Calorim. 111, 1197–1202. https://doi.org/10.1007/s10973-012-2290-x.

Gondard, C., Nadal, M.H., Hennerel, C., 1998. Three ultrasonic devices for the elastic moduli determination at high temperatures. Rev. Prog. Quant. Nondestr. Eval. l7, 867–874. https://doi.org/10.1007/978-1-4615-5339-7_112.

González-Morán, Carlos O., Miranda-Hernández, José G., Agustín Flores Cuautle, José de Jesús, Suaste-Gómez, Ernesto, Herrera-Hernández, Héctor, 2017. A PLZT novel sensor with Pt implanted for biomedical application: cardiac micropulses detection on human skin. Ann. Mater. Sci. Eng. 2017, 1–7. https://doi.org/10.1155/2017/2054940.

Granados, L., Moreno, V., Vieira, L.E., Escobar, J.A., Hotza, D., Novaes de Oliveira, A.P., Rodrigues-Neto, J.B., 2017. Alumina/copper foams produced by replica using a double impregnation process. Adv. Appl. Ceram. 116, 85–91. https://doi.org/10.1080/17436753.2016.1236533.

Hulbert, S.F., Young, F.A., Mathews, R.S., Klawitter, J.J., Talbert, C.D., Stelling, F.H., 1970. Potential of ceramic materials as permanently implantable skeletal prostheses. J. Biomed. Mater. Res. 4, 433–456. https://doi.org/10.1002/jbm.820040309.

Iftekhar, S., Grins, J., Svensson, G., Lööf, J., Jarmar, T., Botton, G.A., Andrei, C.M., Engqvist, H., 2008. Phase formation of $CaAl_2O_4$ from $CaCO_3$-Al_2O_3 powder mixtures. J. Eur. Ceram. Soc. 28, 747–756. https://doi.org/10.1016/j.jeurceramsoc.2007.08.012. doi:.

Jiangling, L., Qifeng, S., Xinmei, H., Kuochih, C., 2015. Effect of TiO_2 addition on crystallization characteristics of CaO-Al_2O_3-based mould fluxes for high Al steel casting. ISIJ Int. 55, 830–836. https://doi.org/10.2355/isijinternational.55.830.

Jifang, X., Jieyu, Z., Chang, J., Lei, T., Kuochih, C., 2012. Measuring and modeling of density for selected CaO-MgO-Al_2O_3-SiO_2 slag with low silica. J. Iron Steel Res. Int. 19, 26–32. https://doi.org/10.1016/S1006706X(12)601095.

Jifang, X., Jieyu, Z., Dong, C., Minqi, S., Wenping, W., 2016. Effects of MgO content and CaO/Al_2O_3 ratio on surface tension of calcium aluminate refining slag. J. Cent. South Univ. 23, 3079–3084. https://doi.org/10.1007/s11771-016-3372-x.

José, G., Miranda, Hernández, Bustamante, M. Vázquez, Herrera Hernández, H., Morán, C.O. González, Rocha Rangel, E., Refugio García, E., 2016. Tenacidad a la fractura de compuestos cermets $3Al_2O_3{\cdot}2SiO_2$/Ag manufacturados por molienda de alta energía. Materia 21https://doi.org/10.1590/S1517-707620160001.0022. 243-25.

JSA - JIS R 1607, 1990. Testing Method for Fracture Toughness of High Performance Ceramics. Japanese Standards Association.

Kalita, S.J., Bose, S., Bandyopadhyay, A., Hosick, H.L., 2002. Porous calcium aluminate ceramics for bone-graft applications. J. Mater. Res. 17. https://doi.org/10.1557/JMR.2002.0442.

Lawn, H.R., R Fuller, E., 1975. Equilibrium pennylike cracks in indentation fracture. J. Mater. Sci. 10, 2016–2024. https://doi.org/10.1007/BF00557479.

Lawn, B.R., Evans, A.G., Marshall, D.B., 1980. Elastic/plastic indentation damage in ceramics: the median/radial crack system. J. Am. Ceram. Soc. 63, 574–581. https://doi.org/10.1111/j.1151-2916.1980.tb10768.x.

Leal Silva, E.J.N., Herrera, D.R., Rosa, T.P., Duque, T.M., Jacinto, R.C., Figueiredo de Almeida Gomes, B.P., Zaia, A.A., 2014. Evaluation of cytotoxicity, antimicrobial activity and physicochemical properties of a calcium aluminate-based endodontic material. J. Appl. Oral Sci. 22, 61–67. https://doi.org/10.1590/1678-775720130031.

Ligaszewski, M., Surówka, K., Stekla, J., 2009. The shell features of cornu aspersum (synonym helix aspersa) and helix pomatia: characteristics and comparison. Am. Malacol. Bull. 27, 173–182. https://doi.org/10.4003/006.027.0215.

Loof, J., Engqvist, H., O Ahnfelt, N., Lindqvist, K., Hermansson, L., 2003. Mechanical properties of a permanent dental restorative material based on calcium aluminate. J. Mater. Sci. Mater. Med. 14, 1033–1037. https://doi.org/10.1023/B:JMSM.0000003999.52349.0d.

Lourençoa, R.R., Angélicab, R.S., de Anchieta Rodriguesa, J., 2013. Preparation of refractory calcium Aluminate cement using the sonochemical process. Mater. Res.-Ibero-am. J. Mater. 16, 731–739. https://doi.org/10.1590/S1516-14392013005000041.

Marxen, J.C., Becker, W., Finke, D., Hasse, B., Epple, M., 2003. Early mineralization in Biomphalaria glabrata: microscopic and structural result. J. Molluscan Stud. 69, 113–121. https://doi.org/10.1093/mollus/69.2.113.

Miranda Hernández, J.G., Ortega Avilés, M., Herrera Hernández, H., González Morán, C.O., García Pacheco, G., Rocha Rangel, E., 2018. Refractory ceramics synthesis by solid-state reaction between $CaCO_3$ (mollusk shell) and Al_2O_3 powders. Ceram.-Silik. 62, 355–363. https://doi.org/10.13168/cs.2018.0031.

Miskufova, A., Havlik, T., Bitschnau, B., kielski, A., Pomadowski, H., 2015. Properties of CaO sintered with addition of active alumina. Ceram.-Silik. 59, 115–124. http://www.ceramics-silikaty.cz/index.php?page=cs_detail_doi&id=43.

Moradkhani, A., Baharvandi, H., Tajdari, M., Latifi, H., Martikainen, J., 2013. Determination of fracture toughness using the area of micro-crack tracks left in brittle materials by Vickers indentation test. J. Adv. Ceram. 2, 87–102. https://doi.org/10.1007/s40145-013-0047-z.

Naga, S.M., Hassanb, A.M., El-Maghraby, H.F., Awaad, M., 2019. Characterization of physico- mechanical properties of Alumina/YAG/Ceria composites. Ceram. Int. 45, 1634–1640. https://doi.org/10.1016/j.ceramint.2018.10.040.

Niihara, K., Morena, R., H Hasselman, D.P., 1982. Evaluation of KIC of brittle solids by the indentation method with low crack-to-indent ratios. J. Mater. Sci. Lett. 1, 13–16. https://doi.org/10.1007/BF00724706.

Niju, S., Meera Sheriffa Begum, K.M., Anantharaman, N., 2016. Enhancement of biodiesel synthesis over highly active CaO derived from natural white bivalve clam shell. Arab. J. Chem. 9, 633–639. https://doi.org/10.1016/j.arabjc.2014.06.006.

Oliveira, I.R., Pandolfelli, V.C., Jacobovitz, M., 2010. Chemical, physical and mechanical properties of a novel calcium aluminate endodontic cement. Int. Endod. J. 43, 1069–1076. https://doi.org/10.1111/j.1365-2591.2010.01770.x.

Parreira, R.M., Andrade, T.L., Luz, A.P., Pandolfelli, V.C., Oliveira, I.R., 2016. Calcium aluminate cement-based compositions for biomaterial applications. Ceram. Int. 42, 11732–11738. https://doi.org/10.1016/j.ceramint.2016.04.092.

Pramanick, A.K., 2015. Evaluation of fracture toughness of sintered silica-nickel nanocomposites. Int. J. Renew. Energy Technol. 4, 334–339. https://doi.org/10.15623/ijret.2015.0403057.

Regina de Oliveira, I., Luana de Andrade, T., Parreira, R.M., Jacobovitz, M., Pandolfelli, V.C., 2015. Characterization of calcium aluminate cement phases when in contact with simulated body fluid. Mater. Res.-Ibero-am. J. Mater. 18, 382–389. https://doi.org/10.1590/1516-1439.336714.

Rivas, M.J.M., De Aza, A.H., Pena, P., 2005. Synthesis of CaAl2O4 from powders: particle size effect. J. Eur. Ceram. Soc. 25, 3269–3279. https://doi.org/10.1016/j.jeurceramsoc.2004.06.021.

Rivas Mercury, J.M., De Aza, A.H., Peña, P., 2005. Synthesis of CaAl2O4 from powders: perticle size effect. J. Eur. Ceram. Soc. 25, 3269–3279. https://doi.org/10.1016/j.jeurceramsoc.2004.06.021.

Scrivener, K.L., Cabiron, J.L., Letourneux, R., 1999. Highperformance concretes from calcium aluminate cements. Cement Concr. Res. 29, 1215–1223. https://doi.org/10.1016/S00088846(99)001039.

Sergejev, F., Antonov, M., 2006. Comparative study on indentation fracture toughness measurements of cemented carbides. Proc. Estonian Acad. Sci. Eng 12, 388–398. http://kirj.ee/public/va_te/eng-2006-4-7.pdf.

Shukla, P.P., Lawrence, J., Wu, H., 2010. On the fracture toughness of a zirconia engineering ceramic and the effects thereon of surface processing with fibre laser radiation. J. Eng. Manuf. 224, 1555–1569. https://doi.org/10.13140/RG.2.1.2245.7043.

Singh, A., Purohit, K.M., 2010. Chemical synthesis, characterization and bioactivity evaluation of hydroxyapatite prepared from garden snail (helix aspersa). J. Bioprocess. Biotech. 1, 1–5. https://doi.org/10.4172/2155-9821.1000104.

Smith, A.J., Jackson, M.S., Bagg, J., 2001. The ecology Staphylococcus species in the oral cavity. J. Med. Microbiol. 50, 940–946.

Tahaa, M.A., Nassara, A.H., Zawrah, M.F., 2017. Improvement of wetability, sinterability, mechanical and electrical properties of Al2O3-Ni nanocomposites prepared by mechanical alloying. Ceram. Int. 43, 3576–3582. https://doi.org/10.1016/j.ceramint.2016.11.194.

Tsang, P.C., Chu, F.C., Samaranayake, L.P., 2002. Staphylococci may indeed cause acute dental infections. BMJ 325, 599. http://hdl.handle.net/10722/42611.

Uchida, A., Nade, S.M., McCartney, E.R., Ching, W., 1984. The use of ceramics for bone replacement. A comparative study of three different porous ceramics. Bone Joint Lett. J 66. https://doi.org/10.1302/0301-620X.66B2.6323483.

N. Viriya, P. Krasae, B. Puttasawat, B. Yoosuk, N. Chollacoop, K. Faungnawakij, Waste shells of mollusk and egg as biodisel production catalysts, Bioresour. Technol. 101 3765-3767. doi: 10.1016/j.biortech.2009.12.079.

White, M.M., Chejlava, M., Fried, B., Sherma, J., 2007. The concentration of calcium carbonate in shells of freshwater snails. Am. Malacol. Bull. 22, 139–143. https://doi.org/10.4003/0740-2783-22.1.139.

Wieczorek-Ciurowa, K., Dulian, P., Nosal, A., Domagała, J., 2010. Effects of reagents' nature on mechanochemical synthesis of calcium titanate". J. Therm. Anal. Calorim.

101, 471–477. https://doi.org/10.1007/s10973-010-0802-0.
Yongpan, T., Xiaolin, P., Haiyan, Y., Ganfeng, T., 2016. Formation mechanism of calcium aluminate compounds based on high temperature solid-state reaction. J. Alloy. Comp. 670, 96–104. https://doi.org/10.1016/j.jallcom.2016.02.059.
Zabeti, M., Wan Daud, W.M.A., Aroua, M.K., 2009. Optimization of the activity of CaO/Al_2O_3 catalyst for biodiesel production using response surface methodology. Appl. Catal. A-Gen. 366, 154–159. https://doi.org/10.1016/j.apcata.2009.06.047.
Zawrah, M.F., Khalil, N.M., 2007. Synthesis and characterization of calcium aluminate nanoceramics for new applications. Ceram. Int. 23, 1419–1425. https://doi.org/10.1016/j.ceramint.2006.04.022.